Entropic stochastic resonance of finite-size particles in confined Brownian transport

Hai-Wei Hu,[1,2] Lin Du,[1,2,*] Ai-Li Fan,[1,2] Zi-Chen Deng,[1,2,3,†] and Celso Grebogi[4]

[1]*School of Mathematics and Statistics, Northwestern Polytechnical University, Xi'an 710072, China*

[2]*MIIT Key Laboratory of Dynamics and Control of Complex Systems, Northwestern Polytechnical University, Xi'an 710072, China*

[3]*School of Aeronautics, Northwestern Polytechnical University, Xi'an 710072, China*

[4]*Institute for Complex Systems and Mathematical Biology, Kingdom College, University of Aberdeen, Aberdeen AB24 3UE, United Kingdom*

(Received 10 July 2023; accepted 5 April 2024; published 8 May 2024)

We demonstrate the existence of entropic stochastic resonance (ESR) of passive Brownian particles with finite size in a double- or triple-circular confined cavity, and compare the similarities and differences of ESR in the double-circular cavity and triple-circular cavity. When the diffusion of Brownian particles is constrained to the double- or triple-circular cavity, the presence of irregular boundaries leads to entropic barriers. The interplay between the entropic barriers, a periodic input signal, the gravity of particles, and intrinsic thermal noise may give rise to a peak in the spectral amplification factor and therefore to the appearance of the ESR phenomenon. It is shown that ESR can occur in both a double-circular cavity and a triple-circular cavity, and by adjusting some parameters of the system, the response of the system can be optimized. The differences are that the spectral amplification factor in a triple-circular cavity is significantly larger than that in a double-circular cavity, and compared with the ESR in a double-circular cavity, the ESR effect in a triple-circular cavity occurs within a wider range of external force parameters. In addition, the strength of ESR also depends on the particle radius, and smaller particles can induce more obvious ESR, indicating that the size effect cannot be safely neglected. The ESR phenomenon usually occurs in small-scale systems where confinement and noise play an important role. Therefore, the mechanism that is found could be used to manipulate and control nanodevices and biomolecules.

DOI: 10.1103/PhysRevE.109.054110

I. INTRODUCTION

In the 1980s, stochastic resonance (SR) was first proposed to explain the periodiclike alternation between the glacial and warm periods of the glacial climate [1,2], describing a counterintuitive phenomenon, in which, in some nonlinear systems, noise is not always harmful for detecting or transducing an incoming weak signal, and that an appropriate dose of noise can amplify the weak signals. Since then, SR has been observed in various systems in different disciplines such as physics, engineering, and biomedicine [3–12]. It is worth noting that these are SR phenomena that occur in pure energetic potentials. However, in practical systems, the diffusion of particles often occurs in confined regions, which can be modeled by cavities of various shapes. The irregular boundary of the confined region gives rise to an entropic contribution to the potential, which has an important influence on the diffusion of particles [13–16]. Previous studies have shown that entropic rectification and current reversal occur when particles diffuse in a confined channel [17–21]. Similarly, the existence and shape of the boundary of the restricted region would also play an important role in the SR dynamics of the particles [22–27].

Burada *et al.* first studied the SR dynamics of Brownian particles in a dumbbell-shaped channel [22], demonstrating that the irregularities in the form of restricted, curved boundaries in the system under consideration can lead to an entropy barrier and can induce noise-assisted resonance behavior. They defined the SR of Brownian particles in a confined space as entropic stochastic resonance (ESR). Since then, the study of ESR in confined space has attracted extensive interest and attention. These studies mainly focus on analyzing the effects of boundary unevenness [23] and different types of noise on ESR [24–27], ESR induced by applying different forces in the longitudinal and transversal directions [28–31], the double entropic stochastic resonance caused by adding a longitudinal constant static force to the system [32], and ESR in time-varying channels [33,34].

However, most of the studies focus on the ESR of pointlike Brownian particles without considering the size of the particles. In fact, the size of the particles has an important influence on the diffusion of the particles in the confined structure [35–38]. In addition, most of the confined structures are double cavities, and there are few studies on the confined mediums of more than two units, except for the study of ESR in a confined channel with four units [23], trapping particles by ESR under periodic confinement [39], and characterizing stochastic resonance in a triple cavity [40]. These results have confirmed that the nondouble cavities can affect particle capture, transit time, and ESR. Therefore, motivated by this and the extension from pointlike Brownian particles to finite-size Brownian particles, this work investigates the ESR in double- and triple-circular cavities. The noise inside the cavities is Gaussian white noise. Based on the assumption of diffusion equilibrium and dimensionality reduction method, an

*lindu@nwpu.edu.cn

†dweifan@nwpu.edu.cn

effective potential function that describes the influence of cavity boundaries is first proposed. Second, a Brownian dynamics simulation is adopted to calculate the motion trajectories of Brownian particles in these two cavities to obtain the mean sample. Next, an ESR indicator, the spectral amplification, can be obtained by performing Fourier expansion on the average trajectory of particles. Then, the influences of external force parameters on ESR in the double-circular cavity are addressed, including amplitude and frequency of the external force; meanwhile, the ESR phenomena in the these two types of cavities are compared. Finally, the dependence of entropic stochastic resonance on the radius of Brownian particles in a triple-circular cavity is discussed.

The structure of this paper is as follows. The model description and physical theory, including the spectral amplification and method to calculate an ESR indicator, are given in Sec. II. In Sec. III, major results and associated analysis are presented. In Sec. IV, a conclusion of the results ends the paper.

II. MODEL DESCRIPTION AND PHYSICAL THEORY

A. Model of particle diffusion

The dynamics of a Brownian particle in a confined channel subjected to a constant gravity G acting along the transverse direction and a sinusoidal oscillating force $F(t)$ along the axis of the channel can be described by means of the Langevin equation written [41], in the overdamped limit [42], as

$$\gamma_r \frac{d\vec{r}(t)}{dt} = F(t)\vec{e}_x - G\vec{e}_y + \sqrt{\gamma_r k_B T}\vec{\xi}(t), \tag{1}$$

where $\vec{r}(t) = [x(t),\ y(t)]$ is the position of the particle at time t, $\vec{e}_x$ and $\vec{e}_y$ represent the unit vectors along the x and y directions, k_B is the Boltzmann constant, and T refers to the absolute temperature. γ_r denotes the friction coefficient and satisfies the Stokes's law $\gamma_r = 6\pi\upsilon r_p$, which depends on the shear viscosity υ of the fluid and the particle radius r_p. $\vec{\xi}(t) = [\xi_x(t), \xi_y(t)]$ is the white Gaussian noise with zero mean which satisfies the fluctuation-dissipation relation $\langle \xi_i(t)\xi_j(s)\rangle = 2\delta_{ij}\delta(t-s)$ for $i, j = x, y$. The explicit form of the driving force along the x axis is given by $F(t) = A\sin(\sigma t)$, where A is the amplitude and σ is the driving frequency.

B. Brownian transport system with a double- or triple-circular cavity

In the presence of constrained boundary, the Langevin equations (1) should be solved by imposing reflecting (no-flow) boundary conditions at the walls of the channel. For the two-dimensional structure sketched in Fig. 1, the wall of the double-circular cavity is defined by the half width $y_{u1}(x)$,

$$y_{u1}(x) = \begin{cases} \sqrt{{R_1}^2 - (x+l_1)^2}\ , & -X_{u1}^{\max} \leqslant x \leqslant 0 \\ \sqrt{{R_1}^2 - (x-l_1)^2}\ , & 0 < x \leqslant X_{u1}^{\max}, \end{cases} \tag{2}$$

where R_1 represents the radius of a single-circular cavity, a_1 is the half width of the bottleneck, and l_1 denotes the horizontal distance from the bottleneck to the center of the circle; its length is $l_1 = \sqrt{{R_1}^2 - {a_1}^2}$. In addition, $X_{u1}^{\max}$ refers to the maximum position that the pointlike particles can reach along the x direction in the cavity shown in Fig. 1 and its length is $X_{u1}^{\max} = R_1 + l_1$. According to the symmetry of the double-circular cavity, it is clear that the lower boundary function is $y_{l1}(x) = -y_{u1}(x)$. For an incompressible particle of radius r_p inside the cavity, the available space for its center can be described by the effective half width $w_{e1+}(x)$,

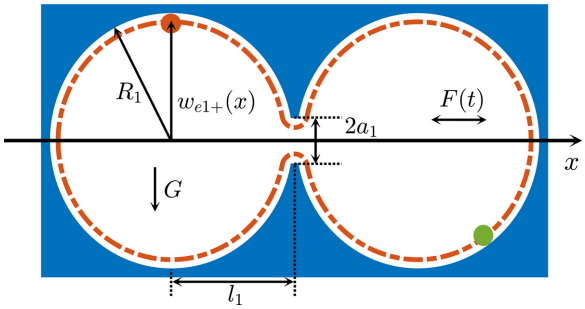

FIG. 1. Sketch of a double-circular cavity, where the forces $F(t)$ and G are applied on the overdamped particles (the orange and green balls in the cavity). The orange dotted line represents the effective boundary that can be reached by the particle center with limited size. The radius of the circular cavity is R_1, and the width of the hole between the two circular cavities is $2a_1$.

$$w_{e1+}(x) = \begin{cases} \sqrt{(R_1 - r_p)^2 - (x+l_1)^2}\ , & -X_{e1}^{\max} \leqslant x < -L_{p1} \\ a_1 - \sqrt{{r_p}^2 - x^2} & , \quad -L_{p1} \leqslant x \leqslant L_{p1} \\ \sqrt{(R_1 - r_p)^2 - (x-l_1)^2}\ , & L_{p1} < x \leqslant X_{e1}^{\max}, \end{cases} \tag{3}$$

where $L_{p1} = l_1 r_p / R_1$ and $X_{e1}^{\max} = R_1 + l_1 - r_p$. In the double-circular cavity depicted in Fig. 1, $X_{e1}^{\max}$ denotes the maximum value that the center of a particle with radius r_p can reach in the x direction. The lower effective boundary is just $w_{e1-}(x) = -w_{e1+}(x)$, and $2w_1(x) = w_{e1+}(x) - w_{e1-}(x)$ gives the local width of the channel accessible for the center of a hard particle with radius r_p. The choice of this structure is intended to resemble the classical setup for stochastic resonance (SR) in the context of energetic barriers. When the gravity G is sufficiently large, the diffusion region of all particles will be very close to the lower boundary of the channel, recovering the effect of an energetic bistable potential.

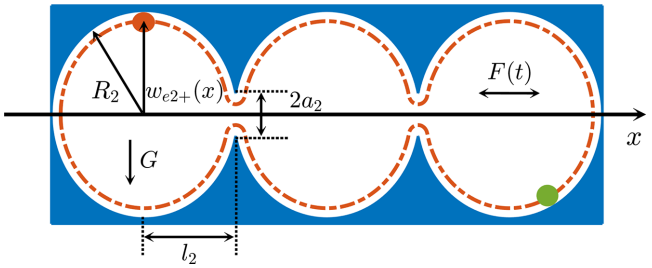

FIG. 2. Sketch of a triple-circular cavity, where the forces $F(t)$ and G are applied on the overdamped particles (the orange and green balls in the cavity). The orange dotted line represents the effective boundary that can be reached by the particle center with limited size. The radius of the circular cavity is R_2, and the width of the hole between two adjacent circular cavities is $2a_2$.

For the two-dimensional structure sketched in Fig. 2, the wall of the triple-circular cavity is defined by the half width $y_{u2}(x)$,

$$y_{u2}(x) = \begin{cases} \sqrt{{R_2}^2 - (x+2l_2)^2}\ , -X_{u2}^{\max} \leqslant x \leqslant -l_2 \\ \sqrt{{R_2}^2 - x^2}\qquad\quad , -l_2 < x \leqslant l_2 \\ \sqrt{{R_2}^2 - (x-2l_2)^2}\ , l_2 < x \leqslant X_{u2}^{\max}, \end{cases} \tag{4}$$

where R_2, a_2, l_2, and $X_{u2}^{\max}$ have the same meanings as those in the double-circular cavity. In the triple-circular cavity depicted in Fig. 2, R_2 represents the radius of a single-circular cavity, a_2 is the half width of the bottleneck, and l_2 denotes the horizontal distance from the bottleneck to the center of the circle; its length is $l_2 = \sqrt{{R_2}^2 - {a_2}^2}$. $X_{u2}^{\max}$ also represents the maximum value that the pointlike particles can reach in the x direction, and there is $X_{u2}^{\max} = R_2 + 2l_2$. In addition, the lower boundary function of the triple-circular cavity is $y_{l2}(x) = -y_{u2}(x)$. For an incompressible particle of radius r_p inside the cavity, the available space for its center can be described by the effective half width $w_{e2+}(x)$,

$$w_{e2+}(x) = \begin{cases} \sqrt{(R_2 - r_p)^2 - (x+2l_2)^2},\ -X_{e2}^{\max} \leqslant x < -(L_{p2} + l_2) \\ a_2 - \sqrt{{r_p}^2 - (x+l_2)^2}, -(L_{p2} + l_2) \leqslant x \leqslant -(l_2 - L_{p2}) \\ \sqrt{(R - r_p)^2 - x^2}, -(l_2 - L_{p2}) < x \leqslant l_2 - L_{p2} \\ a_2 - \sqrt{{r_p}^2 - (x-l_2)^2}, l_2 - L_{p2} \leqslant x \leqslant l_2 + L_{p2} \\ \sqrt{(R_2 - r_p)^2 - (x-2l_2)^2}, l_2 + L_{p2} < x \leqslant X_{e2}^{\max}, \end{cases} \tag{5}$$

where $L_{p2} = l_2 r_p / R_2$ and $X_{e2}^{\max} = R_2 + 2l_2 - r_p$. Similar to the double-circular cavity, the lower effective boundary of the triple-circular cavity drawn in Fig. 2 is $w_{e2-}(x) = -w_{e2+}(x)$.

For the sake of a dimensionless description, we henceforth rescale all lengths in units of $L_R = R$, i.e., $\hat{x} = x/L_R$, $\hat{y} = y/L_R$, implying $\hat{a} = a/L_R$, $\hat{y}_{u1} = y_{u1}/L_R = -\hat{y}_{l1}$, $\hat{y}_{u2} = y_{u2}/L_R = -\hat{y}_{l2}$, $\hat{w}_{e1+} = \omega_{e1+}/L_R = -\hat{w}_{e1-}$, and $\hat{w}_{e2+} = \omega_{e2+}/L_R = -\hat{w}_{e2-}$. We measure time in units of $\tau = \gamma_{\max} L_R^2 / k_B T_R$, where T_R, as a reference temperature, is an arbitrary fixed temperature, i.e., $\hat{t} = t/\tau$ and $\hat{\sigma} = \sigma\tau$. There is $\gamma_{\max} = 6\pi\upsilon a$ in the expression of τ, where a is the maximum radius of particles that can pass through the pores in the confined space. So the friction coefficient of the Brownian particles with radius r_p is given by $\gamma_r = r\gamma_{\max}$, where $r = r_p/a$ is the ratio of the particle radius with radius r_p to the bottleneck half width a, and there is $0 < r \leqslant 1$. We scale forces by $F_R = \gamma_r L_R/\tau$, i.e., the longitudinally acting, sinusoidal force reads $\hat{F}(\hat{t}) = F(t)/F_R$ and the orthogonal force reads $\hat{G} = G/F_R$. In the following, we shall omit the tilde symbols for better legibility. In dimensionless form, the Langevin equation (1) reads

$$\frac{d\vec{r}(t)}{dt} = F(t)\vec{e}_x - G\vec{e}_y + \sqrt{D}\vec{\xi}(t), \tag{6}$$

where we define $D = T/T_R r$.

There are two assumptions, i.e., that the particle density is dilute and the fluid viscosity is strong, which guarantee that all relevant hydrodynamics caused by particle-particle interactions and wall-particle interactions are small and can be safely neglected.

C. Reduction of dimensionality

Since there are reflection boundary conditions at the boundary of the diffusion channel, it is very difficult to derive the x coordinate $x(t)$ and y coordinate $y(t)$ of Brownian particles analytically. Therefore, assuming that the diffusion of particles in the y direction reaches an equilibrium state, we reduce the dimension of the diffusion problem based on this assumption [43,44].

At first, we consider the case in the absence of the periodic forcing, i.e., $F(t) = 0$. Then, the two-dimensional (2D) diffusion dynamics is described by the following 2D Smoluchowski equation [45,46]:

$$\frac{\partial}{\partial t}P(x,y,t) = D\frac{\partial}{\partial x}e^{-U(x,y)/D}\frac{\partial}{\partial x}e^{U(x,y)/D}P(x,y,t) + D\frac{\partial}{\partial y}e^{-U(x,y)/D}\frac{\partial}{\partial y}e^{U(x,y)/D}P(x,y,t), \tag{7}$$

with reflecting boundary conditions at the channel walls and where the potential function is given by $U(x,y) = Gy$. Since we are mainly concerned with the dynamic behavior of Brownian particles in the x direction in this diffusion system, we introduce the marginal probability density function $P(x,t)$, which is obtained by integration over the transverse coordinate,

$$P(x,t) = \int_{-w_{ei+(x)}}^{w_{ei+(x)}} P(x,y,t)dy, \tag{8}$$

where $w_{ei+}(x)$ $(i = 1, 2)$ represents the effective upper boundary of the double-circular cavity $(i = 1)$ or triple-circular cavity $(i = 2)$.

On integrating Eq. (7) over the transverse direction, we get

$$\frac{\partial}{\partial t}P(x,t) = D\frac{\partial}{\partial x}\int_{-w_{ei+}(x)}^{+w_{ei+}(x)}\left[e^{-U(x,y)/D}\frac{\partial}{\partial x}e^{U(x,y)/D}P(x,y,t)\right]dy. \tag{9}$$

Assuming local equilibrium in the y direction, we define the x-dependent effective energy function $A_i(x)$ $(i = 1, 2)$ (omitting

irrelevant constants) reading

$$e^{-A_i(x)/D} = \int_{-w_{ei+}(x)}^{+w_{ei+}(x)} e^{-U(x,y)/D} dy. \tag{10}$$

Consequently, from Eq. (10), one can get the normalized probability distribution, i.e., $\rho(y|x)$, reading

$$\rho(y|x) = e^{-U(x,y)/D} e^{A_i(x)/D}, \tag{11}$$

where $\rho(y|x)$ represents the conditional local equilibrium probability density of y at a given x. Therefore, the 2D probability distribution $P(x, y, t)$ can be approximately expressed as

$$P(x, y, t) \cong P(x, t)\rho(y|x). \tag{12}$$

By substituting Eq. (12) into Eq. (9), the one-dimensional Fokker-Planck equation describing the evolution of particle probability density can be obtained, and the specific expression is

$$\frac{\partial}{\partial t}P(x,t) \cong D\frac{\partial}{\partial x}e^{-A_i(x)/D}\frac{\partial}{\partial x}e^{A_i(x)/D}P(x,t). \tag{13}$$

When $F(t) \equiv 0$ and the particle is subjected to gravity in the negative direction along the y axis, the potential function $U(x, y) = Gy$. By substituting $U(x, y) = Gy$ into Eq. (10), we get

$$\begin{aligned} e^{-A_i(x)/D} &= \int_{-w_{ei+}(x)}^{+w_{ei+}(x)} e^{-Gy/D} dy \\ &= \frac{2D}{G}\frac{e^{Gw_{ei+}(x)/D} - e^{-Gw_{ei+}(x)/D}}{2} \\ &= \frac{2D}{G}\sinh\left(\frac{Gw_{ei+}(x)}{D}\right). \end{aligned} \tag{14}$$

Taking logarithms on both sides of Eq. (14), we get the expression of potential function $A_i(x)$ as

$$A_i(x) = -D\ln\left[\frac{2D}{G}\sinh\left(\frac{Gw_{ei+}(x)}{D}\right)\right]. \tag{15}$$

Then, Eq. (13) can be rewritten as

$$\frac{\partial P(x,t)}{\partial t} = \frac{\partial}{\partial x}\left[D\frac{\partial P(x,t)}{\partial x} + A'_i(x)P(x,t)\right], \tag{16}$$

where $A_i(x)$ is given by Eq. (15) and the prime refers to the derivative with respect to x. In general, after the coarse graining, the diffusion coefficient will depend on the coordinate x, but since in our case $\langle w'_{ei+}(x)^2\rangle \ll 1$, the correction can be safely neglected [47,48]. For a 2D structure shown in Fig. 1, the free energy $A_1(x)$ is expressed as a double-well potential; cf. Fig. 3. Similarly, for the triple-circular cavities depicted in Fig. 2, $A_2(x)$ forms a triple-well potential; cf. Fig. 4. Therefore, Eq. (16) describes the motion of a Brownian particle in a bistable or tristable potential of entropic nature. It is important to highlight that the potential function $A_i(x)$ does not only depend on the energetic contribution of the gravity G, but also on the temperature D and the geometry of the double- or triple-circular cavity in a nontrivial way. When the small hole connecting two adjacent circular cavities disappears, i.e., $a_i = 0 (i = 1, 2)$, the particles cannot diffuse into another circular cavity, and stochastic resonance will not occur. It should be emphasized that the bistable or tristable potential function does not exist in the two-dimensional Langevin equations, but arises due to the entropic restrictions associated to the confinement of the channel boundary.

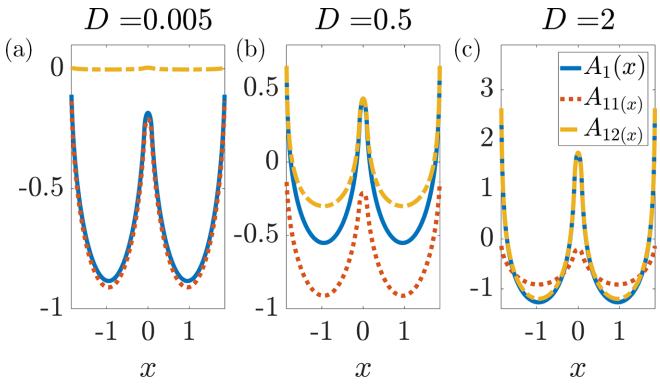

FIG. 3. Schematic diagram of effective potential function $A_1(x)$ and effective potential functions $A_{11}(x)$ and $A_{12}(x)$ under two limit cases when three different noise intensities D are taken in the double-circular cavity.

For potential function $A_i(x)$, there are two limiting cases, which can be obtained by changing the value of the ratio between the energy associated to the transversal force G and the thermal energy D. When $Gw_{ei+}(x)/D \gg 1$, it can be obtained from Eq. (15) that the potential function $A_i(x)$ turns into $A_i(x) \approx -Gw_{ei+}(x) = A_{i1}(x)$ (neglecting irrelevant constants), which means that the boundary of the confined space, $w_{ei+}(x)$, acts as a double- or triple-well potential under the action of gravity G; cf. Figs. 3 and 4. At the same time, as shown in Figs. 3(a) and 4(a), when the thermal energy D is very small ($D = 0.005$), $Gw_{ei+}(x)/D \gg 1$ is satisfied and the effective potential function $A_i(x)$ (solid blue line) is completely consistent with $A_{i1}(x)$ (dotted orange line). In this energy-dominated case, the 1D Fokker-Planck equation (16) becomes

$$\frac{\partial P(x,t)}{\partial t} = \frac{\partial}{\partial x}\left[D\frac{\partial P(x,t)}{\partial x} - Gw'_{ei+}(x)P(x,t)\right], \tag{17}$$

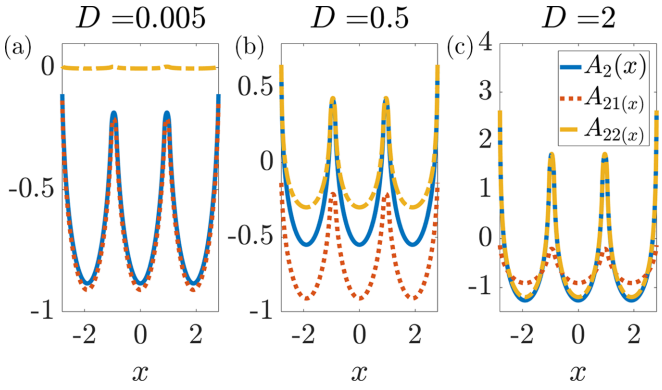

FIG. 4. Schematic diagram of effective potential function $A_2(x)$ and effective potential functions $A_{21}(x)$ and $A_{22}(x)$ under two limit cases when three different noise intensities D are taken in the triple-circular cavity.

which describes the diffusion of Brownian particles in a pure energy potential. When $Gw_{ei+}(x)/D \ll 1$, the potential function $A_i(x)$ can be approximately rewritten as $A_i(x) \approx -D\ln[2w_{ei+}(x)] = A_{i2}(x)$, which implies that the effective potential function $A_i(x)$ is dominated by the purely entropic contribution. In Figs. 3(c) and 4(c), the thermal energy D is set to $D = 2$. When $Gw_{ei+}(x)/D \ll 1$ is established, it can be seen that the potential functions $A_i(x)$ (solid blue line) and $A_{i2}(x)$ (yellow dash-dotted line) are consistent. In this entropy-dominated case, Eq. (16) turns into

$$\frac{\partial P(x,t)}{\partial t} = \frac{\partial}{\partial x}\left[D\frac{\partial P(x,t)}{\partial x} - D\frac{w'_{ei+}(x)}{w_{ei+}(x)}P(x,t)\right], \tag{18}$$

which is a Fick-Jacobs equation [43,49].

D. Spectral amplification

In the case of Brownian particles diffusing in a double-circular cavity, it is instructive to analyze the occurrence of stochastic resonance in the context of the two-state approximation. For a potential $A(x)$ with barrier height ΔA, the escape rate of an overdamped Brownian particle from one cavity to the other in the presence of thermal noise, and in the absence of a force, is given by the overdamped Kramers rate [50–52], reading

$$r_K(D) = \frac{\sqrt{A''(x_{\min})|A''(x_{\max})|}}{2\pi}\exp\left(\frac{-\Delta A}{D}\right), \tag{19}$$

where $A''(x)$ is the second derivative of the effective potential function, and with $x_{\max}$ and $x_{\min}$ indicating the position of the maximum and minimum of the potential, respectively. The expression of barrier height is $\Delta A = A(x_{\max}) - A(x_{\min})$. For the potential given by Eq. (15) and the shape defined by Eq. (3), the corresponding Kramers rate for transitions from one basin to the other, in dimensionless units, reads

$$r_K(D) = \frac{G\sqrt{\sinh\left[\frac{2G(R_1-r_p)}{D}\right]\sinh\left(\frac{2Ga_1}{D}\right)}}{4\pi\sqrt{r_p(R_1-r_p)^3\sinh^2\left[\frac{G(R_1-r_p)}{D}\right]}}. \tag{20}$$

The occurrence of stochastic resonance can be detected in the spectral amplification η. It is defined by the ratio of the power stored in the response of the system at frequency σ and the power of the driving signal [3,53,54], and reads

$$\eta = \frac{1}{D^2}\frac{4r_K^2(D)}{4r_K^2(D)+\sigma^2}. \tag{21}$$

In the presence of an oscillating force $F(t)$ in the x direction, there is an additional contribution to the effective potential function in Eq. (15). We define the new effective potential function as $V(x)$ and its expression is

$$\begin{aligned} V(x) &= A(x) - F(t)x \\ &= -D\ln\left[\frac{2D}{G}\sinh\left(\frac{Gw_{ei+}(x)}{D}\right)\right] - F(t)x. \end{aligned} \tag{22}$$

Thus, the 1D kinetic equation turns into

$$\frac{\partial P(x,t)}{\partial t} = \frac{\partial}{\partial x}\left\{D\frac{\partial P(x,t)}{\partial x} + [A'(x) - F(t)]P(x,t)\right\}. \tag{23}$$

In order to study the appearance of stochastic resonance, one can analyze the response of the system to the applied sinusoidal signal $F(t)$ in terms of the spectral amplification η. By spatial discretization, using a Chebyshev collocation method, and employing the method of lines, the 1D kinetic equation (23) can be reduced to a system of ordinary differential equations. Then, Eq. (23) can be solved using a backward differentiation formula method. With this approach, the probability density distribution varying with time $P(x,t)$ can be obtained. Next, the time-dependent average position of particles $\langle x(t)\rangle$ can be solved, and its expression is defined as

$$\langle x(t)\rangle = \int xP(x,t)\,dx. \tag{24}$$

In the long-time limit, this mean position of particles $\langle x(t)\rangle$ approaches the periodicity of the external driving force [53] with angular frequency σ. After a Fourier expansion of $\langle x(t)\rangle$, one can get the amplitude M_σ of the first harmonic of the output signal. Hence, the spectral amplification η [54] for the fundamental oscillation reads

$$\eta = \left[\frac{M_\sigma}{A}\right]^2. \tag{25}$$

It can be seen from Eq. (25) that the key to solving the spectral amplification η by the numerical simulation method is to obtain the output signal $\langle x(t)\rangle$, i.e., the time-dependent average position of particles. Since the diffusion of Brownian particles in the confined cavity is described by Eq. (1), and there are reflection boundary conditions at the wall, the Brownian dynamics simulation method can be used to simulate the diffusion process of Brownian particles. By simulating a large number of sample paths for a long time, many time-dependent positions of particles $x(t)$ can be obtained. After averaging them, one can get the mean value $\langle x(t)\rangle$, and then the spectral amplification η can be calculated according to the above method.

III. RESULTS AND ANALYSIS

At first, we fix the basic parameters of the restricted channels. The radius of the double- and triple-circular cavity is $R_i = 1$ $(i = 1, 2)$, the half width of the hole connecting adjacent units is $a_i = 0.3R_i$, and the radius of particles in the channel is taken as $r_p = 0.3a_i$.

A. ESR in double-circular cavity

Figure 5 depicts the change of the spectral amplification η with the noise intensity D when the driving signal frequencies are $\sigma = 0.01, 0.001$, and 0.0001. The results shown by the three solid lines in Fig. 5 are obtained from Eq. (21), which is the analytical expression for calculating the spectral amplification η derived by the two-state approximation. The results indicated by three different types of symbols in Fig. 5 are obtained by numerically integrating the one-dimensional probability density equation (23) to obtain the output signal $\langle x(t)\rangle$, which is then calculated by Eq. (25) after Fourier transformation. The amplitude of the periodic signal set here is $A = 10^{-3}$. It can be seen from Fig. 5 that the spectral amplification η presents a nonmonotonic change trend with the increase of

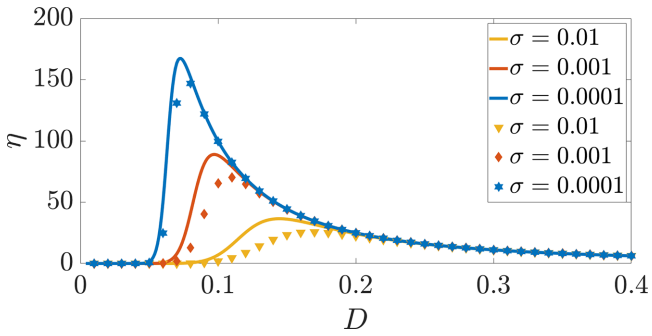

FIG. 5. Schematic diagram of the change of spectral amplification η with noise intensity D when taking different periodic driving signal frequencies σ ($\sigma = 0.01, 0.001, 0.0001$), for the input signal amplitude $A = 10^{-4}$, the transversal force $G = 1$, and for the radius of double-circular cavity $R_1 = 1$. For small driving frequencies and amplitudes, the spectral amplification η is calculated by the two-state approximation and Brownian dynamics simulation. The corresponding results of the solid lines with different colors are obtained by the two-state approximation, i.e., Eqs. (19)–(21), while the corresponding results of the symbols with different shapes are calculated by Brownian dynamics simulation.

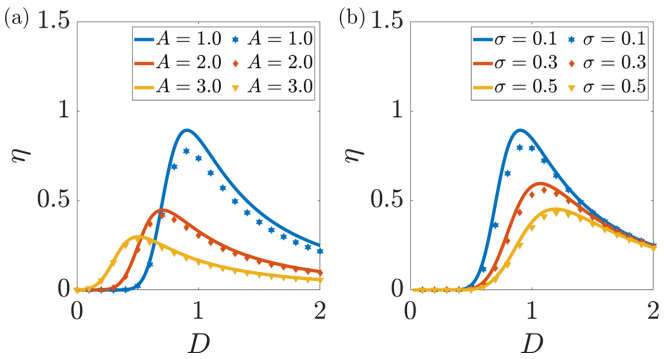

FIG. 6. (a) The dependence of the spectral amplification η on noise intensity D when different amplitudes A ($A = 1.0, 2.0, 3.0$) are taken, for the transversal force $G = 5.5$ and the periodic driving signal frequency $\sigma = 0.1$. (b) The dependence of spectral amplification η on noise level D at three different input signal frequencies σ ($\sigma = 0.1, 0.3, 0.5$), at a constant input amplitude $A = 1.0$ and transversal force $G = 5.5$. Different from the driving frequencies σ and amplitudes A in Fig. 5, for larger σ and A, the spectral amplification η is calculated by the one-dimensional modeling and Brownian dynamics simulation. The solid line corresponds to the result of numerical integration through the one-dimensional probability density equation (23), and different types of symbols are marked as the results obtained by the Brownian dynamics simulation method.

noise intensity D. There is an optimal noise intensity D to maximize the spectral amplification η, indicating that entropic stochastic resonance occurs in the system at this time. When the frequency of the periodic signal is $\sigma = 0.0001$, the results obtained by the two methods are in good agreement. When the frequency of the periodic signal is large, that is, $\sigma = 0.001$ and $\sigma = 0.01$, the results obtained by the two methods have the same trend, but the specific results are in poor agreement, which indicates that the two-state approximation has a good description for the diffusion system with small amplitude and frequency of the driving signal.

When there is a large amplitude and frequency of the driving signal in the diffusion system, the output signal $\langle x(t)\rangle$ can be solved by numerical integration of Eq. (23) and Brownian dynamics simulation, respectively, and the spectral amplification η can be calculated according to Eq. (25) after Fourier transformation of $\langle x(t)\rangle$.

Figure 6(a) describes the curve of spectral amplification η versus noise intensity D when different amplitudes A of the periodic driving signal is taken under the condition of gravity $G = 5.5$ and periodic driving signal frequency $\sigma = 0.1$. The solid line in Fig. 6(a) corresponds to the results of numerical integration through the one-dimensional probability density equation (23), and different symbols correspond to the results of numerical simulation using the Brownian dynamics simulation method. The two results are in good agreement. It can be seen from the change trend of the curve that the spectral amplification η shows a nonmonotonic change behavior with the noise intensity D. When three different amplitude parameters A are taken, the spectral amplification η has a peak value, indicating that the entropic stochastic resonance phenomenon occurs at this time. The peak value of the spectral amplification η and the corresponding noise intensity D decrease with the increase of the amplitude A of the periodic driving signal, indicating that the larger the amplitude A is, the smaller the noise intensity required for entropic stochastic resonance to occur, and the less obvious the entropic stochastic resonance phenomenon is. It can also be found from Fig. 6(a) that under the condition of weak noise, the larger the amplitude A of the periodic driving signal is, the larger the spectral amplification η is. When the noise intensity increases to a critical value, this magnitude relationship will reverse.

Figure 6(b) shows the change of spectral amplification η with noise intensity D when taking different frequencies σ of the periodic driving signal under the condition of gravity $G = 5.5$ and amplitude $A = 1.0$ of the periodic driving signal. It can be seen from Fig. 6(b) that under the three sets of signal frequency parameters that are taken, the spectral amplification η shows a nonmonotonic change trend. When the noise intensity D is appropriate, the spectral amplification η reaches the peak, which indicates that entropic stochastic resonance occurs in the diffusion system at this time. When gravity G and external signal amplitude A are fixed, with the increase of periodic driving signal frequency σ, the peak value of spectral amplification η becomes smaller and smaller, and the entropic stochastic resonance phenomenon becomes less and less obvious, which indicates that small signal frequency σ is more likely to induce entropic stochastic resonance in the system.

B. ESR in triple-circular cavity, and comparison of ESR in triple- and double-circular cavities

In this part, a triple-circular cavity with the same scale as the double-circular cavity for a given set of R_i and a_i is constructed, as shown in Fig. 2. The spectral amplification η in both cavities has been shown in Fig. 7, which is helpful to compare the similarities and differences of their ESR.

Figure 7 depicts relations between the spectral amplification η and noise intensity D for different values of A, σ,

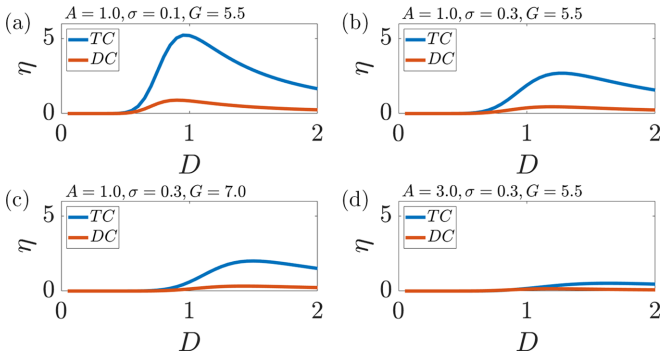

FIG. 7. The dependence of spectral amplification η on noise level D in the triple-circular cavity (TC) and the double-circular cavity (DC) at different external force parameters (including transversal force G, input signal amplitude A, and frequency σ). For the double- and triple-circular cavities, the radius of the cavity, R_i $(i = 1, 2)$, and the half width of the hole connecting adjacent circular cavities a_i are the same, which are $R_i = 1$ and $a_i = 0.3R_i$, respectively. The radius of the Brownian particles diffused in the two cavities is $r_p = 0.3a_i$.

and G in the triple- and double-circular cavities. First of all, according to the value of the spectral amplification η in Fig. 7, it can be seen that η for the triple-circular cavity is much larger than that for the double-circular cavity. This phenomenon can be explained by the jump of Brownian particles in the two cavities. For the same moderate noise intensity D (such as $D = 0.8$), Brownian particles keep a regular jump between different units in both cavities. In the double-circular cavity, however, one Brownian particle jumps to the widest position (near ± 1, as shown in Fig. 1) of a unit and diffuses in a small range. After a period of time, it jumps back and moves around. Finally, after ensemble averaging the trajectories of these Brownian particles, it appears as a periodic function with an amplitude around 1. Then, for the triple-circular cavity, the Brownian particles also maintain a regular jump between different units. Most Brownian particles cross the intermediate unit and jump directly from one side unit to the other side unit. After that, the particles move in a small range near the widest position (near ± 2, as shown in Fig. 2) of the unit they located, and then jump back after a while. Therefore, after ensemble averaging, the average trajectory of these Brownian particles is a periodic function with an amplitude smaller than 2 but much larger than 1, which leads to a larger η in the triple-circular cavity. Second, in Figs. 7(a) and 7(b), the $\eta - D$ curve for the two circular cavities has a peak, which indicates the occurrence of ESR. It is obvious that the peak value of η in the triple-circular cavity is larger, which indicates that a triple-circular structure is more conducive to inducing stronger ESR for circular cavities with the same radius R_i and half width of the hole connecting adjacent units a_i. Furthermore, the noise intensity D corresponding to the occurrence of ESR in the triple-circular cavity and double-circular cavity is different. Based on Figs. 7(a) and 7(b), in the double-circular cavity, ESR occurs when D is taken as 0.9 and 1.2, respectively. For the triple-circular cavity, ESR occurs at a larger D (near 0.95 and 1.25, respectively). In Fig. 7(c), it can be seen that there is a peak value for η in the triple-circular cavity, which means the occurrence of ESR, but η in the double-circular cavity shows a monotonically increasing trend and there is no peak, i.e., there is no ESR. Figure 7(c) describes a phenomenon that for some of the same A, σ, and G, ESR does not occur simultaneously in both triple- and double-circular cavities. Figure 7(c) also illustrates that the range of system parameters that can induce ESR in the triple-circular cavity considered here is wider than that in the double-circular cavity. According to Fig. 7(d), it can be seen that there is no peak for η in both triple- and double-circular cavities, indicating that for some certain parameter conditions, ESR cannot occur in both circular cavities.

Although the intensity of ESR in the triple- and double-circular cavities is different, there are still some common rules regarding ESR in these two types of cavities. In Figs. 7(a) and 7(b), when σ changes from 0.1 to 0.3, both η and its peak in the two circular cavities decrease, indicating that an increase in σ will lead to a decrease in η and a weaker ESR. Similarly, in Figs. 7(b) and 7(c), when G changes from 5.5 to 7.0, η and its maximum in these two circular cavities decrease, i.e., an increase of G leads to a smaller η and weaker ESR. The difference is that even though the increase in G leads to a weakening of ESR in the triple-circular cavity, ESR still exists, while ESR disappears in the double-circular cavity, indicating that ESR in the triple-circular cavity can appear within a wider range of parameters related to G. In Figs. 7(b) and 7(d), the influence of A on ESR in these two circular cavities is presented. The simulation results show that an increase of A can cause a decrease of η and the disappearance of ESR in these two types of cavities.

Overall, for the triple- and double-circular cavities given in Figs. 2 and 1, the results indicate that only increasing the number of circular cavity units can enable the ESR effect to occur within a wider range of external force parameters. In addition, an increase in the number of cavity units can also lead to the increase of the spectral amplification η and its peak, i.e., the more pronounced ESR effect can be induced.

C. ESR of Brownian particles with different radii in triple-circular cavity

The Brownian particles that diffuse in a confined space are of finite size, and the factor of particle size cannot be ignored in many cases. Particles with different sizes are subject to different constraints from the channel boundary, and the entropic barrier is also different; therefore, particles of different sizes may have different diffusion velocities, diffusion coefficients, etc., which directly or indirectly affects the entropic stochastic resonance of particles. In this part, we focus on particle size by fixing other parameters and study the entropic stochastic resonance phenomenon of Brownian particles with different sizes in a three-circular cavity, as shown in Fig. 2. The diffusion of particles in the cavity is governed by Eq. (6). The values of transverse force G, input signal amplitude A, and frequency σ of the input signal are consistent with those in Fig. 7(a), which are $G = 5.5$, $A = 1.0$, and $\sigma = 0.1$.

Figure 8 describes in detail the variation of the spectral amplification factor η with the noise intensity D for four different sizes of Brownian particles. It can be understood from Fig. 8 that the spectral amplification factor η shows a nonmonotonic trend with the noise intensity D, and there is a peak demonstrating that ESR occurs in the system. We define

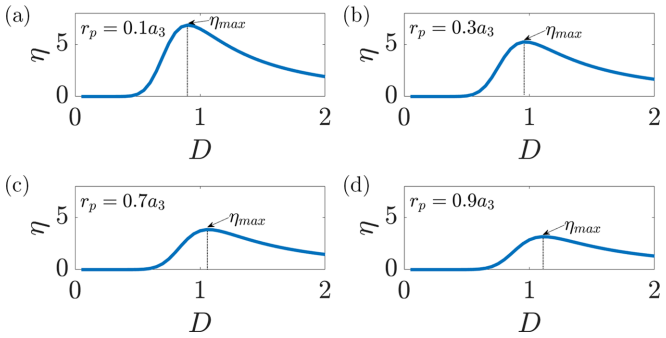

FIG. 8. The dependence of spectral amplification η of Brownian particles of different sizes on noise level D in the triple-circular cavity (TC) with the same external force parameters (including transversal force G, input signal amplitude A, and frequency σ). In the four subgraphs, the radii of the Brownian particles diffused in the cavity are $0.1a_3$, $0.3a_3$, $0.7a_3$, $0.9a_3$, respectively.

the maximum value of the spectral amplification factor η as $\eta_{\max}$, which can represent the strength of ESR in the system. By comparing the $\eta_{\max}$ values of four different particle sizes in Fig. 8, it can be seen that the larger the radii of Brownian particles, the smaller the value of $\eta_{\max}$, indicating that the ESR is weaker.

Figure 9 shows the dependence of the maximum value of spectral amplification $\eta_{\max}$ on particle radius r_p in the triple-circular cavity (TC). It can be seen that $\eta_{\max}$ decreases monotonously with the increase of particle radius r_p. The smaller the particle radius is, the larger the value of $\eta_{\max}$ is, which indicates that the ESR is more pronounced. As the size of the Brownian particle increases, the value of $\eta_{\max}$ begins to decrease and the ESR in the system becomes weaker and weaker. In particular, when the particle radius is $r_p > a_3$, this means that the radius of the particle, r_p, exceeds the half width of the channel pore a_3, the particle will be limited to a certain cavity, unable to diffuse from one cavity in the channel to another cavity, and the ESR phenomenon will not occur.

In summary, the ESR of Brownian particles of different sizes has been studied in a triple-circular cavity. It has been shown that the smaller the radius of a particle, the more noticeable ESR is. The strength of ESR in the system has a strong dependence on the particle radius. Therefore, the size effect is an important feature that cannot be neglected in the study of such problems.

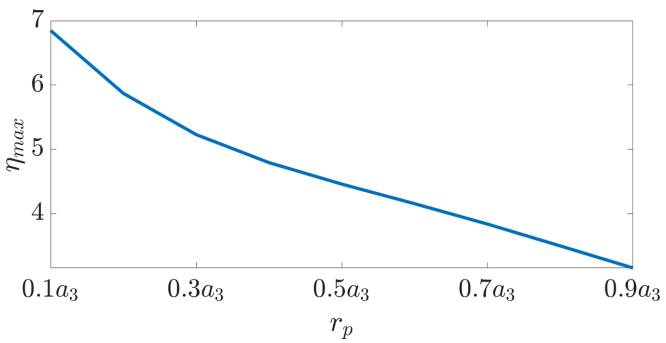

FIG. 9. The dependence of the maximum value of spectral amplification $\eta_{\max}$ on particle radius r_p in the triple-circular cavity (TC). The external force parameters (including transversal force G, input signal amplitude A, and frequency σ) are consistent with those in Fig. 8.

IV. CONCLUSION

We have studied the phenomenon of entropic stochastic resonance in double- and triple-circular cavities. In a double-circular cavity, the two-state approximation method has been shown to be suitable for calculating the spectral amplification for small input signal amplitudes and frequencies. By calculating the spectral amplification η numerically, influences of the external force parameters on ESR are explored. The spectral amplification shows a nonmonotonic trend with the noise level. When the noise intensity is appropriate, the spectral amplification reaches the peak, which means that ESR occurs.

Meanwhile, the influence of a triple-circular cavity structure on ESR is studied, and phenomena that are different from ESR in a double-circular cavity with same cavity radius and the same pore width as the triple-circular cavity are presented. Interestingly, the triple-circular structure of confinements can induce a larger maximum in the η versus D curve, which indicates that there is more obvious ESR in a triple-circular cavity. In addition, ESR does not simultaneously occur in a double-circular cavity and a triple-circular cavity. When some external force parameters are taken, ESR only occurs in a triple-circular cavity, but not in a double-circular cavity. The triple-circular cavity can induce a wider parameter region that can induce the maximum and ESR, but does not affect the trend of the spectral amplification induced by external forces.

Finally, by simulating the diffusion of four different sizes of Brownian particles in the triple-circular cavity, the curves of the spectral amplification factor with noise intensity are obtained. It can be seen that the particle radius size is also an important factor affecting the ESR phenomenon. We learn that the smaller the particle size, the higher the peak value of the spectral amplification factor, corresponding to a more remarkable ESR phenomenon. Consequently, in many. micro- and nanoscale systems, the size effect of particles is an important attribute affecting the response of the system, which cannot be safely omitted.

Our results show the dependence of ESR and the noise intensity that induces ESR on the external force parameters and the structure of confinements, which provides the possibility for a design of stylized channels wherein response and transport become efficiently optimized.

ACKNOWLEDGMENTS

This work was supported by the National Natural Science Foundation of China (NNSFC, Grants No. 12172291 and No. 11972292), Shaanxi Province Outstanding Youth Fund Project (Grant No. 2024JC-JCQN-05) and the 111 Project (Grant No. BP0719007).

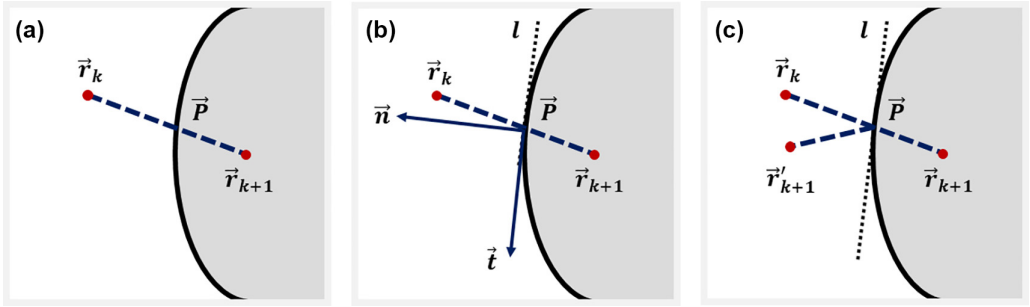

FIG. 10. Realization of reflection boundary conditions. (a) Check whether the particles move outside the channel. (b) Calculate the collision point, and the tangent vector and normal vector at the collision point when the particles diffuse outside the channel. (c) Calculate the new position coordinates of the particles after collision with the wall according to the reflection boundary condition.

APPENDIX: BROWNIAN DYNAMICS SIMULATION

When the particle diffuses in a confined space, the space where the particle is located has a boundary limit. When the particle collides with the obstacle, the size and direction of the particle diffusion velocity will change. The boundary in Figs. 1 and 2 is the reflection boundary. The particle and the obstacle completely elastically collide. After the rebound, the particle is without energy loss, the diffusion velocity remains unchanged, and the diffusion direction is similar to the specular reflection, as shown in Fig. 10. Because the particle is considered to diffuse in a low Reynolds number fluid environment, the interaction between the particles is ignored here.

Let $\vec{r}_k = (x_k, y_k)$ denote the position of the particle at time $(k-1)h$, where h refers to the time step. The reflection boundary condition, i.e., updating the particle position from Fig. 10(a) to Fig. 10(b) at each time step, is implemented according to the following algorithm:

(1) Set the initial position of the particle $\vec{r}_1 = (x_1, y_1)$.

(2) Update the position $\vec{r}_{k+1} = (x_{k+1}, y_{k+1})$ of the particle at time kh according to Eq. (6) and determine whether the position of the particle is in the confined media. If $\vec{r}_{k+1} = (x_{k+1}, y_{k+1})$ is located in the restricted space, the position $\vec{r}_{k+2} = (x_{k+2}, y_{k+2})$ of the particle is continuously updated according to Eq. (6); otherwise, steps (3)–(6) are performed.

(3) Calculate the intersection point $\vec{P} = (x_p, y_p)$ between the boundary and the line from $\vec{r}_k$ to $\vec{r}_{k+1}$, where $\vec{r}_k = (x_k, y_k)$ represents the position of the particle at time $(k-1)h$.

(4) Calculate the tangent line l at the intersection point $\vec{P} = (x_p, y_p)$, and calculate the tangent unit vector $\vec{t}$ and the normal unit vector $\vec{n}$ (outgoing from the wall), as shown in Fig. 10(b).

(5) Calculate the position point $\vec{r}'_{k+1} = (x'_{k+1}, y'_{k+1})$ after the collision according to the reflection boundary condition, where the calculation formula is $\vec{r}'_{k+1} = \vec{r}_{k+1} - 2[(\vec{r}_{k+1} - \vec{P}) \cdot \vec{n}]\vec{n}$.

(6) Assign the coordinates of the reflection point $\vec{r}'_{k+1} = (x'_{k+1}, y'_{k+1})$ to $\vec{r}_{k+1} = (x_{k+1}, y_{k+1})$, and determine the positional relationship between the new $\vec{r}_{k+1}$ and the channel. If the new $\vec{r}_{k+1}$ is in the restricted space, return to step (2). Otherwise, assign the coordinates of $\vec{P}$ to $\vec{r}_k$, repeat steps (3)–(6) until the reflection point inside the confined space is calculated, and then return to step (2) to continue to update the position of the particle.

The Brownian dynamics simulation requires that the time step h is small enough. If the time step h is too large, it will lead to numerical instability of the particles at some sharp boundaries in the process of numerical simulation, and multiple reflections occur at the sharp boundaries. In addition, the trajectory of the particles may break through the boundary of confined space unnaturally. In order to make the simulation results of Brownian dynamics more accurate, the selected time step h is less than 10^{-4}, and the number of simulated sample orbits is greater than 10^3.

[1] R. Benzi, G. Parisi, A. Sutera, and A. Vulpiani, Tellus **34**, 10 (1982).

[2] R. Benzi, A. Sutera, and A. Vulpiani, J. Phys. A: Math. Gen. **14**, L453 (1981).

[3] L. Gammaitoni, P. Hänggi, P. Jung, and F. Marchesoni, Rev. Mod. Phys. **70**, 223 (1998).

[4] A. R. Bulsara and L. Gammaitoni, Phys. Today **49**(3), 39 (1996).

[5] P. Hänggi, ChemPhysChem **3**, 285 (2002).

[6] J. M. G. Vilar and J. M. Rubí, Phys. Rev. Lett. **77**, 2863 (1996).

[7] J. M. G. Vilar and J. M. Rubí, Phys. Rev. Lett. **78**, 2886 (1997).

[8] V. S. Anishchenko, A. B. Neiman, F. Moss, and L. Shimansky-Geier, Phys. Usp. **42**, 7 (1999).

[9] G. Schmid, I. Goychuk, and P. Hänggi, Europhys. Lett. **56**, 22 (2001).

[10] T. Wellens, V. Shatokhin, and A. Buchleitner, Rep. Prog. Phys. **67**, 45 (2004).

[11] H. Yasuda, T. Miyaoka, J. Horiguchi, A. Yasuda, P. Hänggi, and Y. Yamamoto, Phys. Rev. Lett. **100**, 118103 (2008).

[12] C. Rouvas-Nicolis and G. Nicolis, Scholarpedia **2**, 1474 (2007).

[13] I. Goychuk and P. Hänggi, Phys. Rev. Lett. **91**, 070601 (2003).

[14] I. Goychuk, P. Hänggi, J. L. Vega, and S. Miret-Artés, Phys. Rev. E **71**, 061906 (2005).

[15] D. Reguera, G. Schmid, P. S. Burada, J. M. Rubí, P. Reimann, and P. Hänggi, Phys. Rev. Lett. **96**, 130603 (2006).

[16] S. Martens, G. Schmid, L. Schimansky-Geier, and P. Hänggi, Phys. Rev. E **83**, 051135 (2011).
[17] D. Reguera, A. Luque, P. S. Burada, G. Schmid, J. M. Rubí, and P. Hänggi, Phys. Rev. Lett. **108**, 020604 (2012).
[18] B.-Q. Ai and J.-C. Wu, J. Chem. Phys. **139**, 034114 (2013).
[19] T. Motz, G. Schmid, P. Hänggi, D. Reguera, and J. M. Rubí, J. Chem. Phys. **141**, 074104 (2014).
[20] Y. Li, Y. Xu, W. Xu, Z. Deng, and J. Kurths, Phys. Rev. E **96**, 022152 (2017).
[21] H.-W. Hu, L. Du, L.-H. Qu, Z.-L. Cao, Z.-C. Deng, and Y.-C. Lai, Phys. Rev. Res. **3**, 033162 (2021).
[22] P. S. Burada, G. Schmid, D. Reguera, M. H. Vainstein, J. M. Rubi, and P. Hänggi, Phys. Rev. Lett. **101**, 130602 (2008).
[23] P. S. Burada, G. Schmid, D. Reguera, J. M. Rubi, and P. Hänggi, Eur. Phys. J. B **69**, 11 (2009).
[24] Z. Liang, L. X.-Qin, W. Dan, Z. S.-Qun, and G. J.-Hua, Chin. Phys. Lett. **27**, 040503 (2010).
[25] C.-H. Zeng and H. Wang, Commun. Theor. Phys. **56**, 877 (2011).
[26] L. Du and D. Mei, Eur. Phys. J. B **85**, 75 (2012).
[27] S. Mondal, J. Das, B. C. Bag, and F. Marchesoni, Phys. Rev. E **98**, 012120 (2018).
[28] F. Guo, X.-F. Cheng, and H. Li, Physica A **390**, 3687 (2011).
[29] L. Du, R. Han, J. Jiang, and W. Guo, Phys. Rev. E **102**, 012149 (2020).
[30] J. Jiang, K. Li, W. Guo, and L. Du, Chaos, Solitons Fractals **152**, 111400 (2021).
[31] L. Du, W. Yue, J. Jiang, L. Yang, and M. Ge, Phil. Trans. R. Soc. A. **379**, 20200228 (2021).
[32] P. S. Burada, G. Schmid, D. Reguera, J. M. Rubi, and P. Hänggi, Europhys. Lett. **87**, 50003 (2009).
[33] H. Ding, H. Jiang, and Z. Hou, J. Chem. Phys. **142**, 194109 (2015).
[34] H. Ding, H. Jiang, and Z. Hou, J. Chem. Phys. **143**, 244119 (2015).
[35] W. Riefler, G. Schmid, P. S. Burada, and P. Hänggi, J. Phys.: Condens. Matter **22**, 454109 (2010).
[36] M. Bauer, A. Godec, and R. Metzler, Phys. Chem. Chem. Phys. **16**, 6118 (2014).
[37] M. Bruna and S. J. Chapman, Bull. Math. Biol. **76**, 947 (2014).
[38] Y. A. Makhnovskii, S.-Y. Sheu, D.-Y. Yang, and S. H. Lin, J. Chem. Phys. **146**, 154103 (2017).
[39] N. Shi and V. M. Ugaz, Phys. Rev. E **89**, 012138 (2014).
[40] R. Mei, Y. Xu, Y. Li, and J. Kurths, Philos. Trans. R. Soc. A. **379**, 20200230 (2021).
[41] P. Langevin, C. R. Acad. Sci. (Paris) **146**, 530 (1908).
[42] E. M. Purcell, Am. J. Phys. **45**, 3 (1977).
[43] R. Zwanzig, J. Phys. Chem. **96**, 3926 (1992).
[44] D. Reguera and J. M. Rubí, Phys. Rev. E **64**, 061106 (2001).
[45] P. Hänggi and H. Thomas, Phys. Rep. **88**, 207 (1982).
[46] H. Risken, *The Fokker-Planck Equation: Methods of Solution and Applications*, Springer Series in Synergetics, 3rd ed. (Springer, Berlin, Heidelberg, 1996).
[47] P. S. Burada, G. Schmid, D. Reguera, J. M. Rubí, and P. Hänggi, Phys. Rev. E **75**, 051111 (2007).
[48] P. S. Burada, G. Schmid, P. Talkner, P. Hänggi, D. Reguera, and J. M. Rubí, Biosystems **93**, 16 (2008).
[49] M. H. Jacobs, *Diffusion Processes* (Springer, New York, 1967).
[50] H. A. Kramers, Physica **7**, 284 (1940).
[51] B. McNamara and K. Wiesenfeld, Phys. Rev. A **39**, 4854 (1989).
[52] P. Hänggi, P. Talkner, and M. Borkovec, Rev. Mod. Phys. **62**, 251 (1990).
[53] P. Jung and P. Hänggi, Europhys. Lett. **8**, 505 (1989).
[54] P. Jung and P. Hänggi, Phys. Rev. A **44**, 8032 (1991).